JOURNAL OF SOLID STATE CHEMISTRY 110, 295–304 (1994)

Microstructural Characterization of the $LaNiO_{3-y}$ System

M. J. Sayagués,*,† M. Vallet-Regí,*,‡ A. Caneiro,*,[1] and J. M. González-Calbet*,†,[2]

*Instituto de Magnetismo Aplicado, Apdo. 155, Las Rozas, 28230 Madrid, Spain; †Departamento de Química Inorgánica, Facultad de Químicas, Universidad Complutense, 28040 Madrid, Spain; and ‡Departamento de Química Inorgánica y Bioinorgánica, Facultad de Farmacia, Universidad Complutense, 28040 Madrid, Spain

Received May 7, 1993; in revised form August 2, 1993; accepted August 4, 1993

An electron diffraction and high-resolution electron microscopy study of the $LaNiO_{3-y}$ perovskite-related system shows that compositional variations lead to the formation of new superstructures corresponding to a homologous series of the general formula $La_nNi_nO_{3n-1}$ when $y = 0.5$ and 0.25, i.e., for $n = 2$ and 4, respectively. These members can be described as being formed by ordered intergrowths of $(n-1)$ octahedral layers alternating with one layer in which Ni^{2+} adopts square planar coordination. For different y values, the nonstoichiometry is accommodated by means of disordered intergrowths of octahedral and square-planar layers. © 1994 Academic Press, Inc.

1. INTRODUCTION

As recently reported by Anderson *et al.* (1), many oxygen-deficient perovskites can be described on the basis of more or less complex perovskite-related superstructures of general formula $A_mB_mO_{3m-x}$ or $A_nB_nO_{3n-1}$. This elegant review shows how sizes, electronic configurations, and coordination numbers of A and B cations influence the manner in which layers are stacked. Although most of the 3*d* cations have led to the formation of these ABO_{3-y} phases, nickel has been one of the less studied due to the difficulty in stabilizing mixed oxides of this element with two oxidation states.

In fact, contradictory results have been reported concerning the $La_2Ni_2O_5$ phase where Ni shows formal oxidation state 2+. This material was described by Crespin *et al.* (2) as being monoclinic showing a brownmillerite-type structure, i.e., with one octahedral layer alternating with one tetrahedral layer along the *b*-axis (3). However, Rao and co-workers (4, 5) describe this material on the basis of a tetragonal cell, the oxygen vacancies giving rise to square-planar and octahedral coordination for Ni^{2+}.

In a previous paper (6), we have shown by means of a selected area electron diffraction (SAED) study that a homologous series of the general formula $La_nNi_nO_{3n-1}$ could be described on the basis of $(n-1)$ octahedral layers alternating with one layer showing square-planar coordination. We describe in this paper the synthesis and microstructural characterization by high-resolution electron microscopy (HREM) of $LaNiO_{3-y}$ materials ($y = 0.5$, 0.33, 0.25, and 0.20) where y has been accurately controlled by means of a high-sensitivity thermogravimetric technique.

2. EXPERIMENTAL

Attempts to isolate the $LaNiO_3$ perovskite-related material by the ceramic method have been unsuccessful since a temperature higher than 950°C leads to the stabilization of La_2NiO_4. However, the perovskite-type structure can be stabilized at lower temperature by using a wet method such as the so-called liquid mix technique (7, 8). This technique is based on the formation of metallic complexes from concentrated solutions of polyfunctional organic acids and either salts or oxides of suitable cations for mixed oxide formation. Stoichiometric amounts of $La(NO_3)_3 \cdot 6H_2O$ and $Ni(NO_3)_2 \cdot 6H_2O$, previously analyzed by atomic absorption to determine the cation concentration with an accuracy of 10 ppm, were dissolved in hot citric acid. In order to solidify the liquid solution, ethylene glycol (3% v/v) was added, which increases the solution viscosity. In this way a resin is formed, thus avoiding formation of partial segregation which could modify the homogeneity of the solution. Such a resin was eliminated by heating at 450°C for 16 hr. Then several accumulative treatments were performed until 900°C, where a single phase was obtained. The powder X-ray diffraction pattern of this stoichiometric sample can be indexed on the basis of a rhombohedral cell ($R3m$) with parameters $a = 0.5391(1)$ nm, $\alpha = 60.81(2)°$ (9).

$LaNiO_{3-y}$ ($0.5 \leq y < 0$) materials were obtained by using a thermogravimetric analysis system (TGA) built on the basis of a Cahn D-200 electrobalance which operates under static atmosphere. This system, developed with this aim, consists of the TGA itself coupled to a vacuum and a gas blending system (Fig. 1). A quartz hangdown tube

[1] Permanent address: Centro Atómico Bariloche, 8400 SC Bariloche, Argentina.

[2] To whom correspondence should be addressed.

0022-4596/94 $6.00
Copyright © 1994 by Academic Press, Inc.
All rights of reproduction in any form reserved.

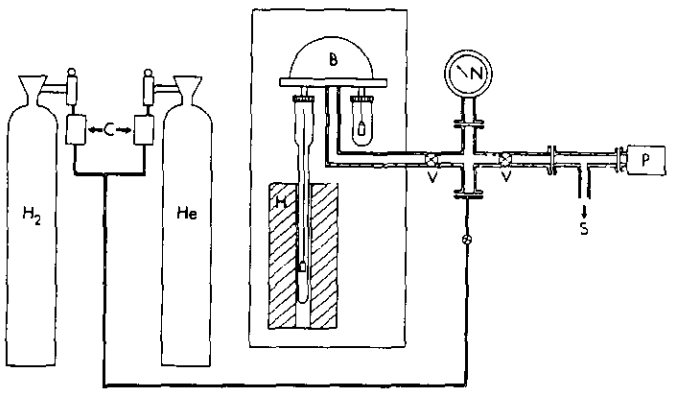

FIG. 1. Thermogravimetric, vacuum, and gas blending system. (C) Mass flow controler; (B) Cahn D-200 electrobalance; (H) furnace; (V) spherical valves; (S) vacuum system; (P) Pirani-Penning.

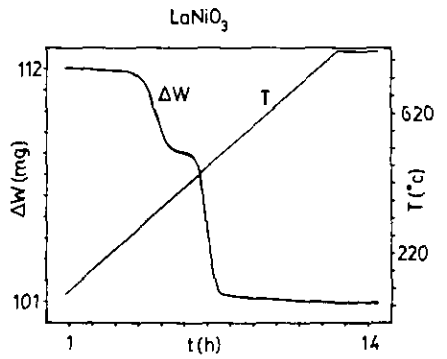

FIG. 2. Weight-loss curve corresponding to the total reduction of $LaNiO_3$.

and an electric furnace permit operating from room temperature to 1000°C and, due to the excellent sensitivity of the electrobalance, the oxygen content can be determined, for instance, within $\pm 2 \times 10^{-3}$ for a $LaNiO_{3-y}$ sample of a total mass of about 100 mg. The vacuum and the gas blending system allow us to operate with a gas mixture at a given total pressure. A H_2/He mixture was used as a reducing atmosphere due to its low density, which reduces hampered effects such as buoyancy and free gas convection.

Mass loss data obtained from temperature-reduced program studies performed at a constant heating rate are used to determine the oxygen content of the starting material as well as the existence of intermediate compounds from a

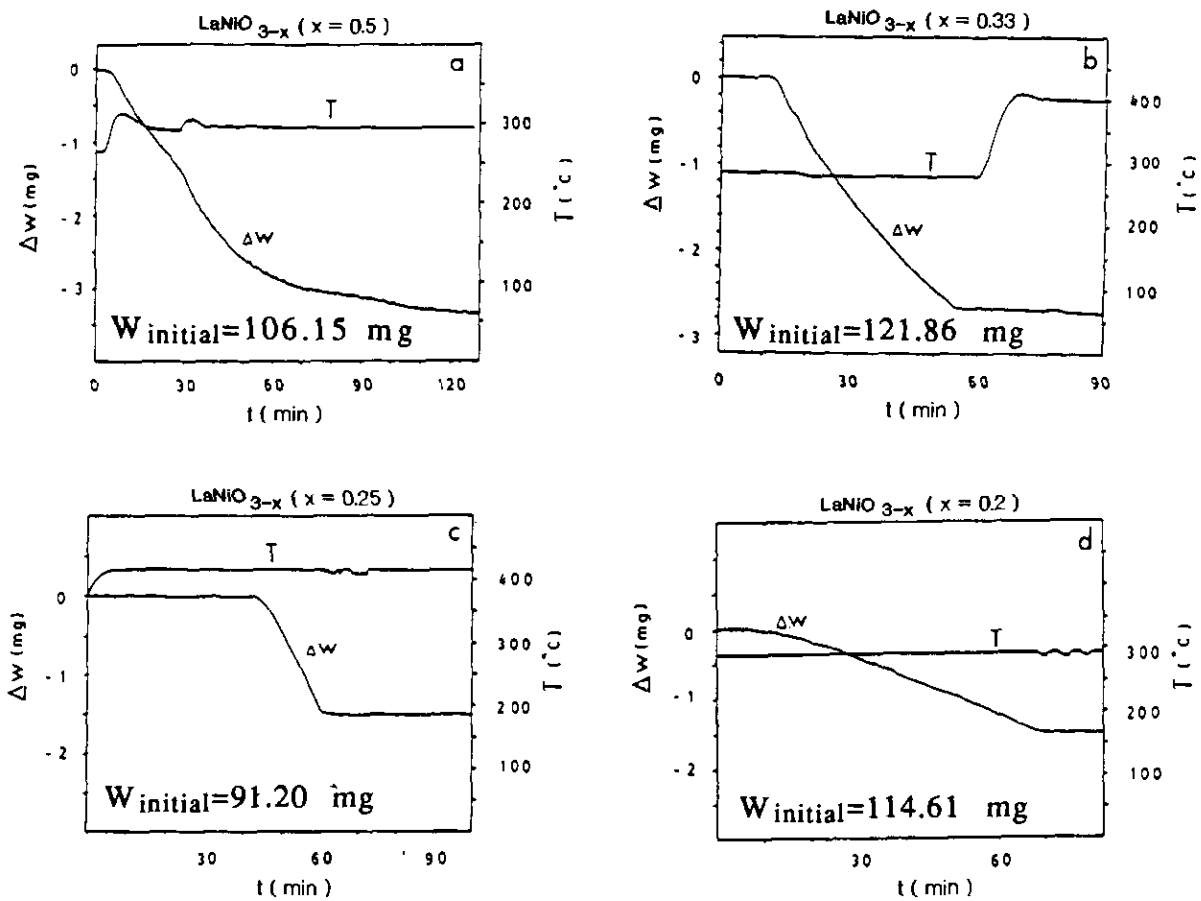

FIG. 3. Weight-loss curves performed to obtain (a) $LaNiO_{2.5}$, (b) $LaNiO_{2.66}$, (c) $LaNiO_{2.75}$, and (d) $LaNiO_{2.8}$.

plateau or inflection point of the so-obtained thermogram. The absolute oxygen content was determined by reducing the samples under a mixture of He/H_2 (0.3 atm/0.2 atm).

Figure 2 shows the weight-loss curve of $LaNiO_3$ as a function of recorded time from room temperature to 800°C. An inflection point for an oxygen content close to $y = 0.5$ is observed, suggesting the existence of a stable phase which could correspond to the member $n = 2$ of the homologous series $La_nNi_nO_{3n-1}$. Unfortunately, the existence of inflection points corresponding to other members of this series was not detected. Therefore, in order to isolate other members of such a family we proceeded as follows. A $LaNiO_3$ sample of approximately 100 mg was heated under vacuum at 200°C in order to eliminate volatile products adsorbed on the sample. Then, a reducing mixture ($0.4He/0.1H_2$ atms) was introduced into the thermobalance and the temperature was raised to 300°C. When the weight loss corresponded to that of the target composition, the gaseous atmosphere was pumped and pure He was introduced. The purge cycle (vacuum and He) was performed several times and, finally, the temperature was raised to 400°C under pure He in order to improve the homogenization of the sample. After 6 hr of such a treatment no appreciable mass change was detected. Figure 3 shows the weight-loss curves and the heating treatment performed for (a) $LaNiO_{2.5}$ ($n = 2$), (b)

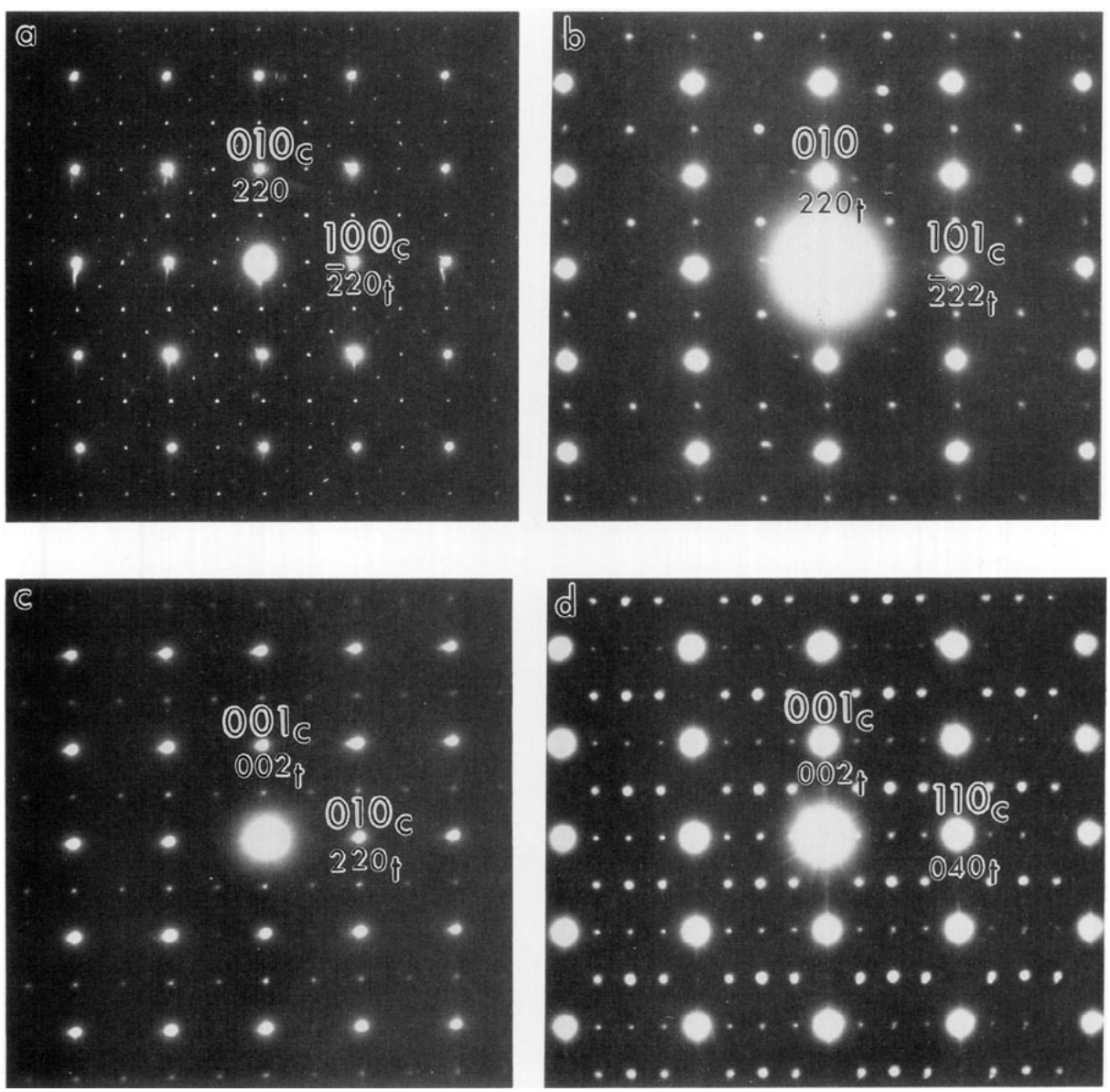

FIG. 4. SAED patterns along the (a) $[001]_t//[001]_c$, (b) $[112]_t//[101]_c$, (c) $[\bar{1}10]_t//[100]_c$, and (d) $[100]_t//[\bar{1}10]_c$ zone axes corresponding to $LaNiO_{2.75}$.

$LaNiO_{2.66}$ ($n = 3$), (c) $LaNiO_{2.75}$ ($n = 4$), and (d) $LaNiO_{2.8}$ ($n = 5$) compositions prepared in this way.

3. RESULTS AND DISCUSSION

3.1. $LaNiO_{2.75}$

The powder X-ray diffraction pattern of this material was indexed on the basis of a triclinic cell with parameters $a = 1.0817(4)$ nm, $b = 1.0895(3)$ nm, $c = 0.7804(3)$ nm, $\alpha = 90.28(2)°$, $\beta = 93.33(1)°$, and $\gamma = 90.29(2)°$.

In order to determine the ordering of oxygen vacancies in this material a SAED and HREM study was performed.

Figure 4a shows a SAED pattern along the $[001]_t//[001]_c$ zone axis (subindexes t and c refer to the triclinic and cubic cells, respectively). The reciprocal angle observed between the $(110)^*_t$ and $(\bar{1}10)^*_t$ is 89.5°, which is coincident with the calculated angle using the triclinic parameters. A fourfold superlattice along $(\bar{1}10)^*_c <> (040)^*_m$ and equivalent reflections, and a twofold superlattice along both perovskite axes are observed. By tilting 45° about the b^* axis, the $[112]_t//[101]_c$ zone axis is obtained (Fig. 4b), where $(010)^*_c$, $(101)^*_c$, and $(111)^*_c$ reflections are doubled.

Figure 4c shows the SAED pattern along $[\bar{1}10]_t//[100]_c$ where weak extra spots are doubling both b^*_c and c^*_c axes. By tilting 45° about the c^* axis, the $[100]_t//[\bar{1}10]_c$ zone axis is obtained (Fig. 4d), a fourfold superstructure appearing again along $[110]_c$.

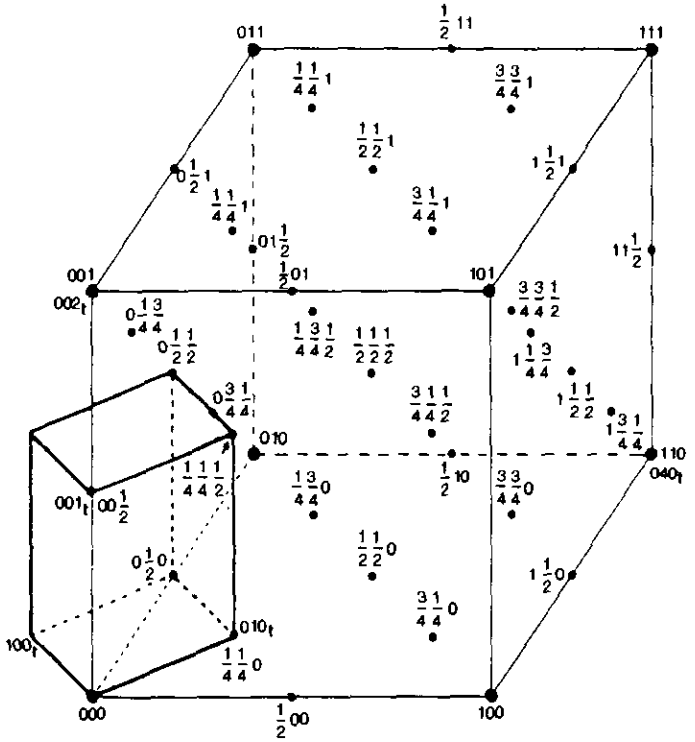

FIG. 5. Schematic representation showing the relationship between the triclinic and pseudocubic reciprocal cells for the $LaNiO_{2.75}$ sample.

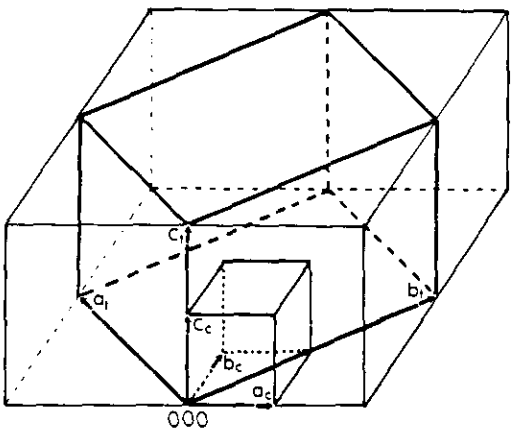

FIG. 6. Schematic representation showing the relationship between the triclinic and pseudocubic real cells corresponding to $LaNiO_{2.75}$.

The diffraction maxima observed allow us to establish the relationship between the triclinic and the cubic reciprocal cells (Fig. 5), according to

$$\begin{aligned} a^*_t &= 1/4[\bar{1}10]^*_c \\ b^*_t &= 1/4[110]^*_c \\ c^*_t &= 1/2[001]^*_c \end{aligned} \quad \begin{pmatrix} a_t \\ b_t \\ c_t \end{pmatrix}^* = \begin{pmatrix} \bar{1}/4 & 1/4 & 0 \\ 1/4 & 1/4 & 0 \\ 0 & 0 & 1/2 \end{pmatrix} \begin{pmatrix} a_c \\ b_c \\ c_c \end{pmatrix}^*.$$

Then, the corresponding relationship between both the triclinic and the cubic real cells is

$$\begin{pmatrix} a_t \\ b_t \\ c_t \end{pmatrix} = \begin{pmatrix} \bar{2} & 2 & 0 \\ 2 & 2 & 0 \\ 0 & 0 & 2 \end{pmatrix} \begin{pmatrix} a_c \\ b_c \\ c_c \end{pmatrix}.$$

The volume of the triclinic cell is 16 times higher than that of the cubic cell (Fig. 6), the relationship with the

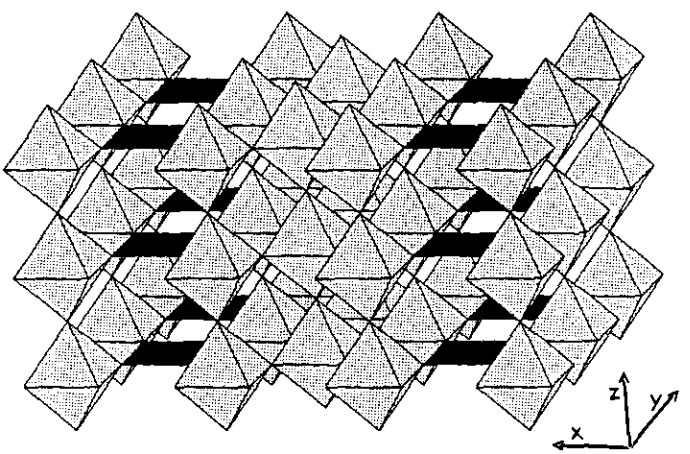

FIG. 7. Structural model proposed for the $LaNiO_{2.75}$ phase.

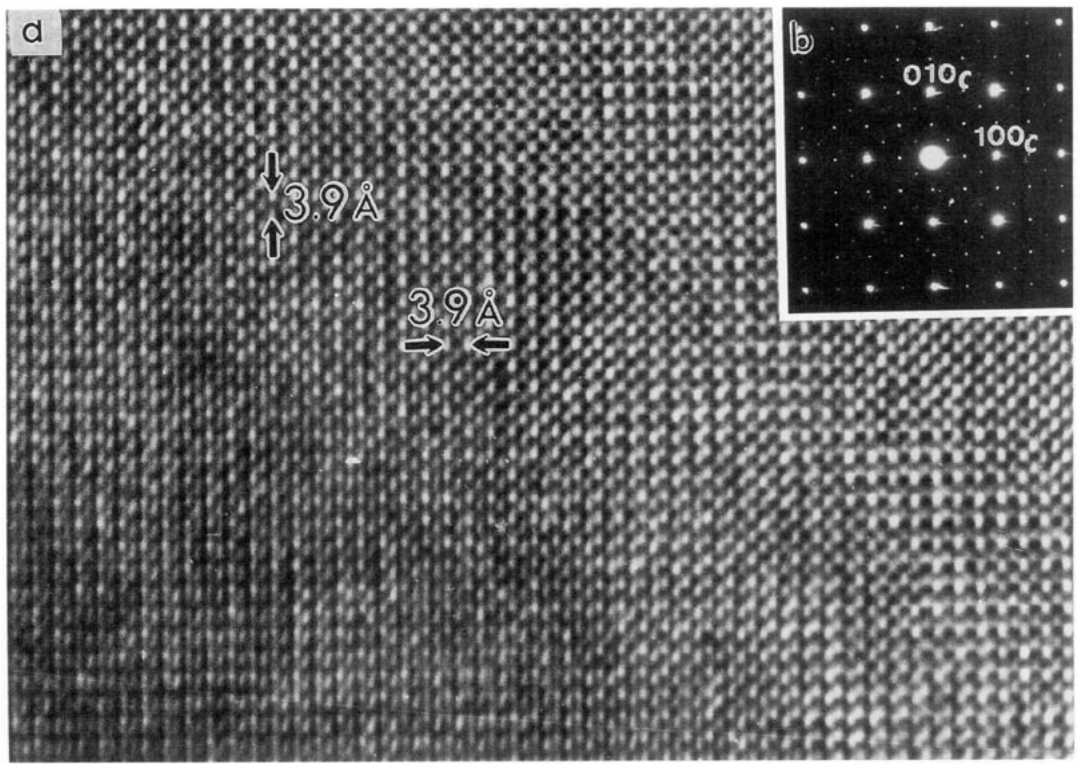

FIG. 8. (a) HREM of an ordered $LaNiO_{2.75}$ crystal along the $[001]_c//[001]_t$ zone axis and (b) corresponding SAED pattern.

cubic perovskite being

$$2a_c\sqrt{2} \times 2a_c\sqrt{2} \times 2a_c, \quad \text{where } a_c = 0.392\ \text{nm},$$

which is in agreement with the powder X-ray diffraction data.

According to this, and taking into account the tendency of Ni to adopt both octahedral and square-planar coordination, a structural model, as shown in Fig. 7, can be proposed, where oxygen vacancies are ordered along the $[110]_c$ direction, leading to $LaO_{0.75}\square_{0.25}$ planes alternating, in an ordered way, with NiO_2 planes along the c-axis. Ni^{3+} shows octahedral coordination (10), while Ni^{2+} should adopt both octahedral (oc) and square planar (sp) coordinations according to the composition $La_4(Ni_2^{3+})_{oc}(Ni^{2+})_{oc}(Ni^{2+})_{sp}O_{11}$.

A HREM micrograph of an ordered $LaNiO_{2.75}$ crystal along $[001]_c//[001]_t$ is shown in Fig. 8. The image contrast was interpreted with the help of a simulation program using the multislice method (11). A series of image calculations along $[001]_c$ (Fig. 9) was carried out, based on the structural model previously shown in Fig. 7, under the following imaging conditions: $C_s = 1$ mm, $C_c = 1.7$ mm, beam divergence angle $= 0.8 \times 10^{-3}$ rad, objective aperture radium $= 0.067\ \text{nm}^{-1}$, accelerating voltage $= 400$ kV, $\Delta f = -30$ to -60 nm and sample thickness (τ) between 1 and 4 nm. It can be observed that a satisfactory agreement

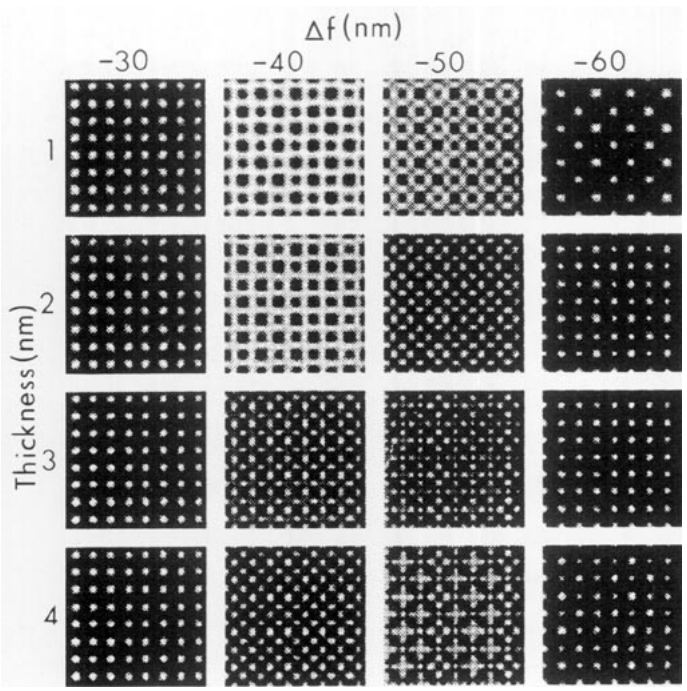

FIG. 9. Through-focus series of calculated crystal-structure images along the $[001]_c$ zone axis corresponding to the $LaNiO_{2.75}$ material.

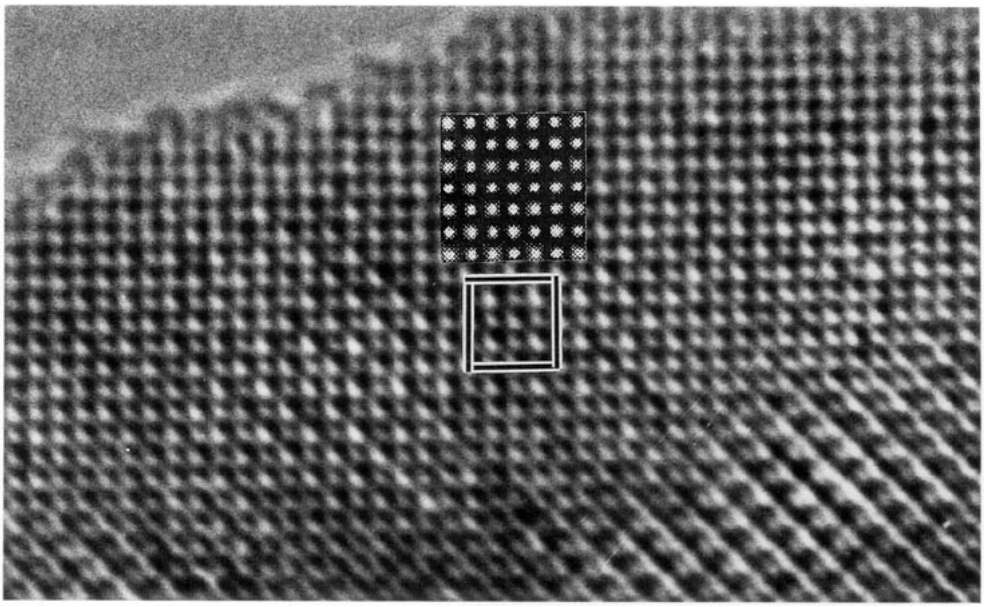

FIG. 10. Experimental and calculated image ($\Delta f = -60$ nm, $\tau = 4$ nm) along the $[001]_c$ zone axis of the $LaNiO_{2.75}$ material.

between experimental and calculated images (Fig. 10) is obtained for the following conditions: $\Delta f = -60$ nm and $\tau = 4$ nm.

On the other hand, it is worth recalling that, for τ values around 1–2 nm, it is possible to elucidate where the anionic vacancies are due to the different image contrast observed in the calculation. Thus, Fig. 11 shows an enlargement of the image calculated at $\Delta f = -40$ nm and $\tau = 1$ nm. It can be observed that following the $[110]_c$ direction, three black dots corresponding to Ni atoms showing similar contrast alternate in an ordered way with a weaker black dot (indicated by arrows). This situation seems to be in agreement with that observed in the structural model where three Ni atoms showing octahedral coordination alternate with a Ni atom in a square-planar site along the $[110]_c$ direction. However, as shown in Figs. 9 and 10, such a difference in the contrast is not detected for higher thickness.

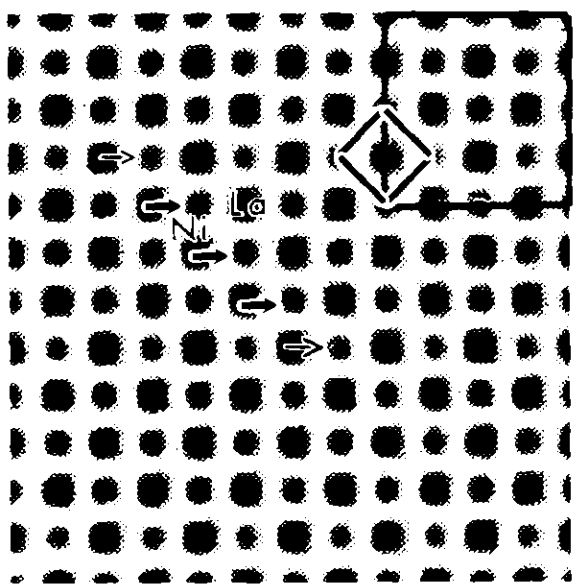

FIG. 11. Enlargement of a calculated image for $LaNiO_{2.75}$ ($[001]_c$; $\Delta f = -40$ nm, $\tau = 1$ nm; 3×3 unit cells). In the top right corner the triclinic and cubic cells are indicated. The arrows show Ni atoms in square-planar coordination every four layers along $[001]_c$.

According to these results, it seems obvious that the new superstructure produced by the ordering of unoccupied oxygen positions cannot be detected in the experimental images where the crystal thickness is between 4 and 10 nm. It is worth mentioning that the HREM image of $LaNiO_3$ along $[001]_c$, i.e., when the perovskite related material shows a fully occupied anionic sublattice, shows the same contrast (Fig. 12) as that observed for $LaNiO_{2.75}$ along the same projection (see Fig. 8). In fact, unoccupied oxygen positions in $La_4Ni_4O_{11}$ are located on the octahedral apex of the perovskite substructure leading to square-planar coordination for the 50% of Ni^{2+}. Regarding the projection of such a structural model along the $[001]_c$ direction (Fig. 13), it can be observed that unoccupied oxygen positions coincide with Ni atoms on the *ab* plane. This seems to explain the difficulty in detecting such differences in the image contrast for thickness higher than 4 nm.

3.2. $LaNiO_{2.5}$

The powder X-ray diffraction pattern of this material was indexed according to Crespin *et al.* (2) on the basis of a monoclinic (m) unit cell with parameters $a =$

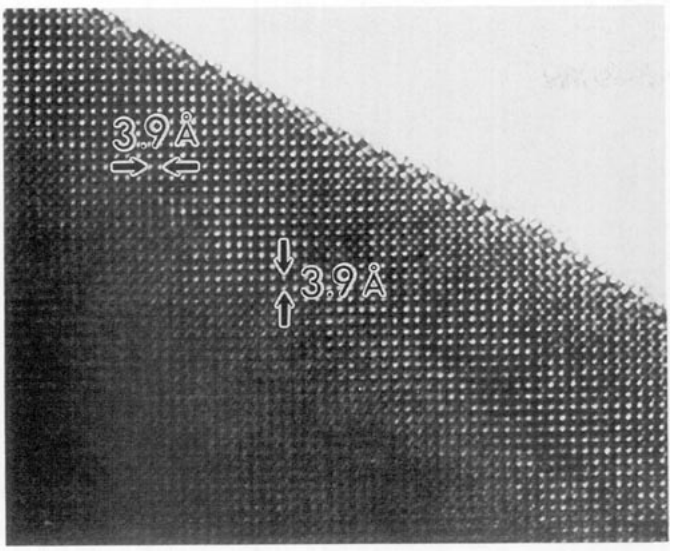

FIG. 12. HREM of $LaNiO_3$ along $[001]_c$.

1.104(1) nm, b = 1.115(1) nm, c = 0.7818(6) nm, and β = 92.19°.

Once again, the SAED study allows us to determine the ordering of oxygen vacancies. Figure 14a shows the SAED pattern along $[010]_m//[110]_c$. The reciprocal angle between $(100)^*_m$ and $(001)^*_m$ reflections is 87.8°, which is in agreement with the monoclinic cell obtained by X-ray diffraction. Weak extra spots corresponding to fourfold and twofold superlattices along $[110]_c$ and $[001]_c$, respectively, can be observed.

By tilting 45° about the c^* axis, the SAED pattern along $[\bar{1}10]_m//[100]_c$ is obtained (Fig. 14b). Extra weak spots at

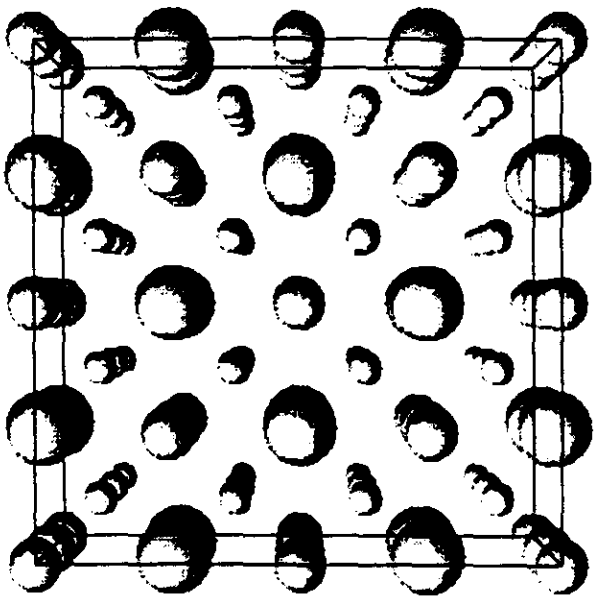

FIG. 13. $[001]_c$ projection of the $La_4Ni_4O_{11}$ structure.

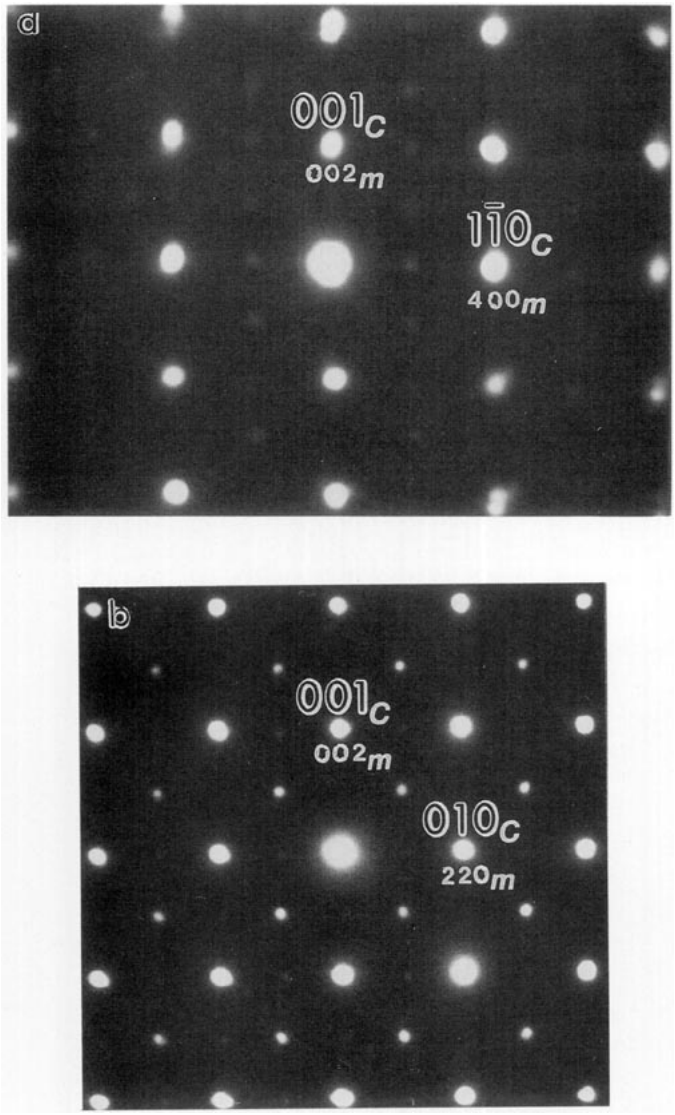

FIG. 14. SAED patterns of $LaNiO_{2.5}$ along (a) $[010]_m//[110]_c$ and (b) $[\bar{1}10]_m//[100]_c$ zone axes.

$(001/2)^*_c$ and $(01/20)^*_c$ and equivalent reflections indicate that c^* and b^* cubic axes are doubled.

Figure 15a shows the SAED pattern along the $[100]_m//[\bar{1}10]_c$ zone axis. A fourfold superlattice along the $[110]^*_c$ direction is seen. By tilting about such a direction the SAED pattern along $[102]_m//[1\bar{1}2]_c$ is obtained (Fig. 15b), where a twofold superlattice along $[\bar{1}11]^*_c$ is observed.

On the basis of this information, a relationship between the monoclinic and the cubic perovskite reciprocal and real cells can be established: $(110)^*_c <> (040)^*_m$, $(\bar{1}10)^*_m <> (400)^*_m$, and $(001)^*_c <> (002)^*_m$; $a_m \sim 2a_c\sqrt{2}$, $b_m \sim 2a_c\sqrt{2}$, and $c_m \sim 2a_c$, being similar to those found for $LaNiO_{2.75}$.

These results seem to indicate that, in agreement with the $La_2Ni_2O_5$ stoichiometry, the most likely structural model can be described (Fig. 16) according to Vidyasagar

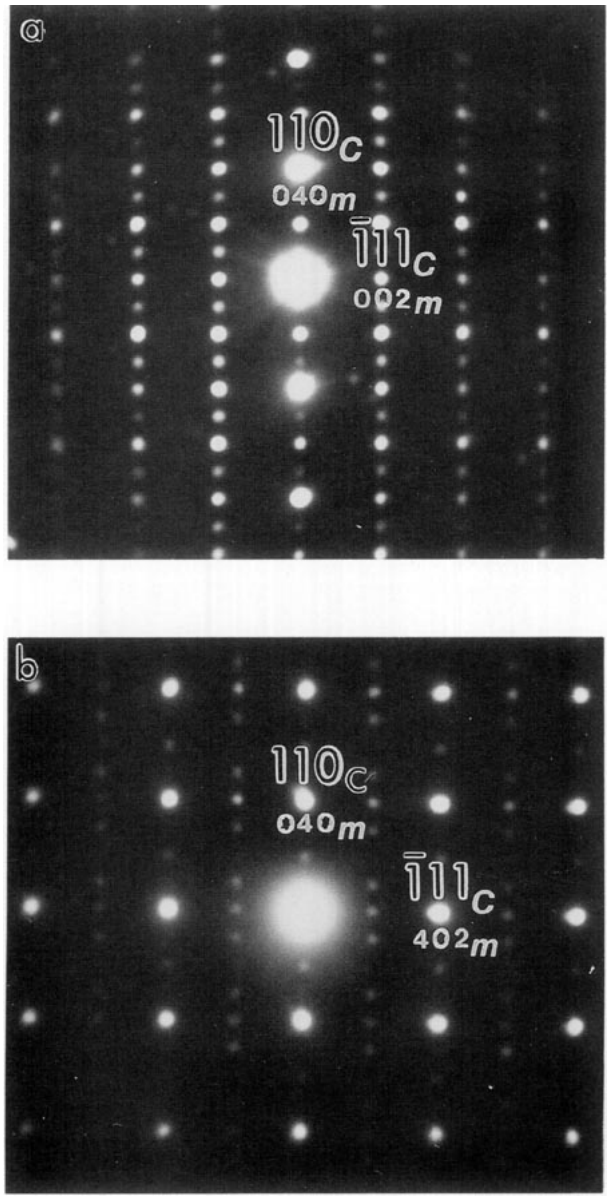

FIG. 15. SAED patterns of $LaNiO_{2.5}$ along (a) $[100]_m//[\bar{1}10]_c$ and (b) $[102]_m//[112]_c$ zone axes.

et al. (4), as formed by an octahedral layer alternating, in an ordered way, with a square-planar layer along the $[100]_c$ direction. However, the cell symmetry is, according to Crespin *et al.* (2), monoclinic, probably due to a tilt of the octahedra.

The HREM image of $La_2Ni_2O_5$ along $[001]_c$ shows the same image contrast as that observed for both $La_4Ni_4O_{11}$ and $LaNiO_3$ along the same direction. Once again, an image calculation was performed on the basis of the structural model depicted in Fig. 16 under the imaging conditions previously described. Similar results were obtained, since only for $\tau \sim 1$–2 nm was it possible to detect contrast differences between Ni atoms in octahedral and square-planar coordination. Figure 17 shows a calculated image

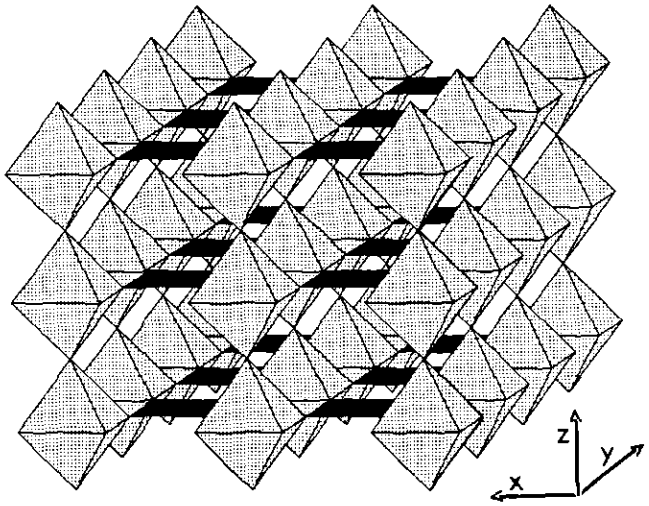

FIG. 16. Structural model proposed for the $La_2Ni_2O_5$.

($\Delta f = -40$ nm, $\tau = 1$ nm), where the different environment of Ni atoms along the $[110]_c$ direction can be observed (marked with arrows).

3.3. *$LaNiO_{2.67}$ and $LaNiO_{2.8}$*

The powder X-ray diffraction patterns of both $LaNiO_{2.67}$ and $LaNiO_{2.8}$ show slightly broad reflections which, in a first approximation, could be indexed on the basis of a monoclinic cell similar to that previously described for $LaNiO_{2.5}$. However, the SAED study shows a somewhat different situation since both $LaNiO_{2.67}$ and $LaNiO_{2.8}$ materials are inhomogeneous.

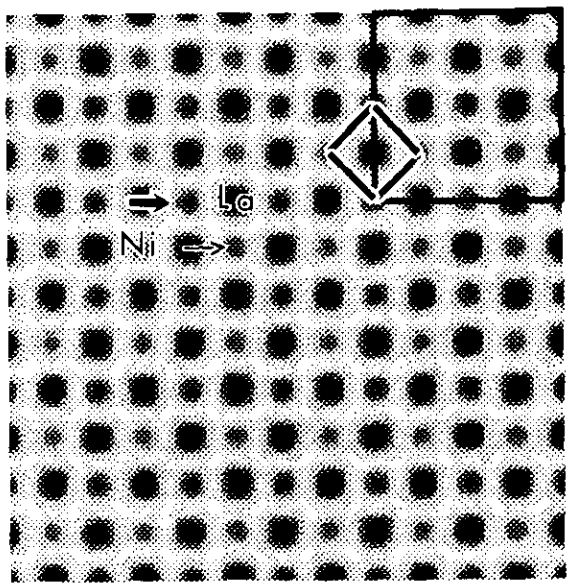

FIG. 17. Calculated image for $LaNiO_{2.5}$ ($[001]_c$; $\Delta f = -40$ nm, $\tau = 1$ nm; 3×3 unit cells). In the top right corner the monoclinic and cubic cells are indicated. The arrows show the contrast difference between Ni atoms in octahedral and square-planar coordination along $[001]_c$.

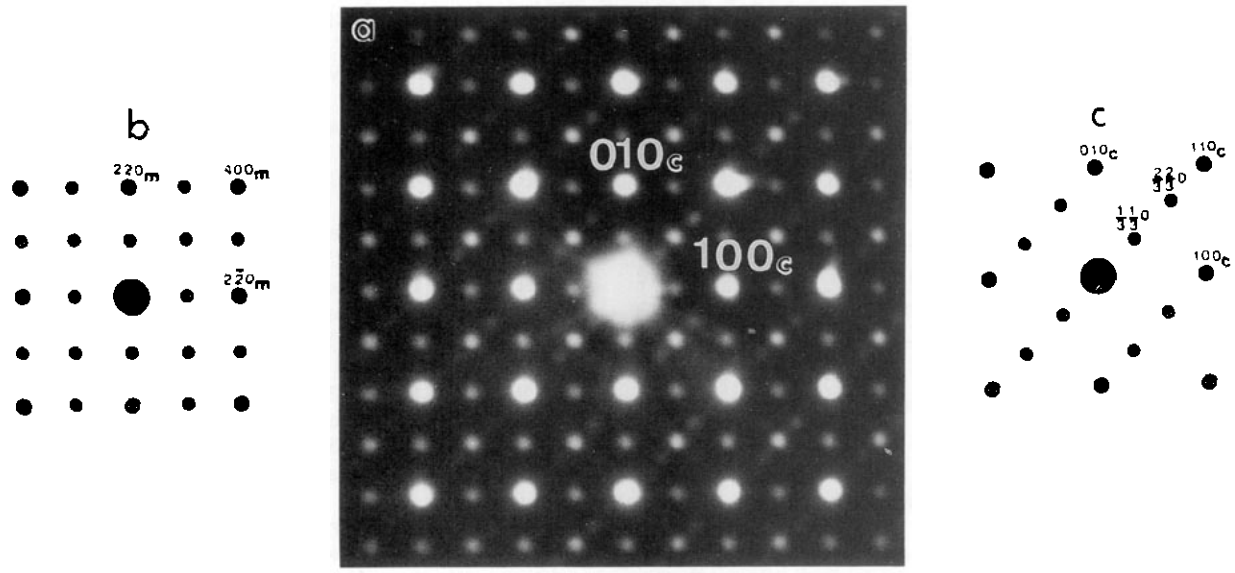

FIG. 18. SAED patterns of $LaNiO_{2.67}$ along the $[001]_m//[001]_c$ zone axis.

Thus, two different kind of crystals were found in $LaNiO_{2.67}$:

—Figure 18a shows the SAED pattern along $[001]_c$ of the first kind of crystals, where the intergrowth of two superlattices along the $[110]_c^*$ direction is observed. One of them, schematized in Fig. 18b, can be indexed on the basis of the unit cell previously proposed for $La_2Ni_2O_5$, along $[001]_m$. The second one, schematized in Fig. 18c, is a threefold superlattice along $[110]_c$. This kind of superstructure reflection seems to indicate that under properly thermodinamic conditions a $La_3Ni_3O_8$ phase could be isolated which, according to previous ideas, could be constituted by two octahedral layers alternating with one square-planar layer along $[110]_c$.

—A second kind of crystals shows, along the same $[001]_c$ zone axis, streaking of the diffraction maxima along both b^* and a^* directions indicative of disorder along such directions.

On the other hand, the SAED study of $LaNiO_{2.8}$ sample shows that the majority of the crystals can be indexed on the basis of the unit cell previously proposed for $LaNiO_{2.75}$ although, in some cases, intergrowth of two- and threefold superlattices were found.

From these results, it seems evident that nonstoichiometry in both $LaNiO_{2.8}$ and $LaNiO_{2.67}$ is accommodated by disordered intergrowth of octahedral and square-planar layers along $[110]_c$.

Taking into account that the composition of these samples corresponds to the hypothetical odd terms of the homologous series $La_nNi_nO_{3n-1}$ ($n = 3, 5$), whereas $LaNiO_{2.5}$ and $LaNiO_{2.75}$ are even terms ($n = 2, 4$), a possible explanation for the difficulty of isolate the odd terms can be found in the comparison of the structural models corresponding to $n = 2$ and $n = 4$ terms with those corresponding to the hypothetical members $n = 3$ and $n = 5$, in which we suppose the anionic vacancies are ordered along $[110]_c$.

Figure 19 shows the different projections along $[001]_c$ corresponding to the structural models of the terms

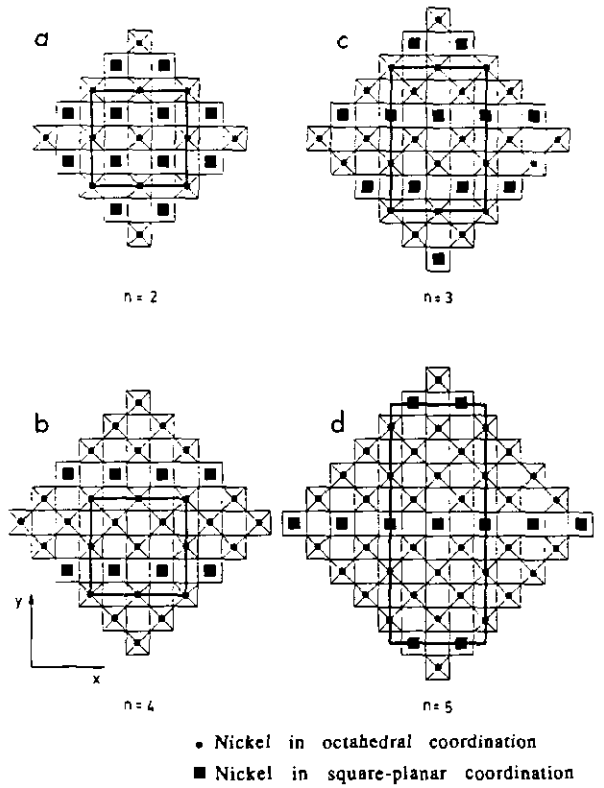

FIG. 19. Structural model of (a) $La_2Ni_2O_5$ ($n = 2$) and (b) $La_4Ni_4O_{11}$ ($n = 4$) along the $[001]_c$ projection; hypothetical model corresponding to (c) $LaNiO_{2.67}$ ($n = 3$) and (d) $LaNiO_{2.8}$ ($n = 5$) along the same projection.

n = 2, 3, 4, and 5. It can be seen that in the case of even terms, the square-planar coordination layers are coincident every n planes. However, for odd members, the periodicity range is longer since the square-planar layers only coincide every $2n$ planes, suggesting that different thermodynamic conditions would be necessary to stabilize them.

These results obtained by SAED and HREM allow us to propose the existence of a homologous series of the general formula $La_nNi_nO_{3n-1}$, where $(n - 1)$ octahedra layers alternate with one square-planar layer along the $[110]_c$ direction. Until now, only the $La_2Ni_2O_5$ (n = 2) and $La_4Ni_4O_{11}$ (n = 4) terms have been isolated.

ACKNOWLEDGMENTS

We acknowledge the C.I.C.Y.T. (Research Projects MAT90-0858-C02-02 and MAT91-0331) for financial support. A. García and E. Baldonedo provided valuable technical assistance.

REFERENCES

1. M. T. Anderson, J. T. Vaughey, and K. R. Poeppelmeier, *Chem. Mater.* **5,** 151 (1993).
2. M. Crespin, P. Levitz, and L. Gatineau, *J. Chem. Soc., Faraday Trans.* **79,** 1181 (1983).
3. E. F. Bertaut, P. Blum, and A. Sagnieres, *Acta Crystallogr.* **12,** 149 (1959).
4. K. Vidyasagar, A. Reller, J. Gopalakrishnan, and C. N. R. Rao, *J. Chem. Soc., Chem. Commun.*, 7 (1985).
5. C. N. R. Rao, J. Gopalakrishnan, K. Vidyasagar, A. K. Ganguly, A. Ramanan, and L. Ganapathi, *J. Mater. Res.* **1,** 280 (1986).
6. J. M. González-Calbet, M. J. Sayagués, and M. Vallet-Regí, *Solid State Ionics* **32/33,** 721 (1989).
7. M. Pechini, *U.S.P.* **3,** 231 (1966).
8. M. Vallet-Regí, E. Garcia, and J. M. González-Calbet, *J. Chem. Soc., Dalton Trans.*, 775 (1988).
9. A. Wold, R. J. Arnolt, and J. B. Goodenough, *J. Appl. Phys.* **29,** 387 (1958).
10. R. D. Shannon, *Acta Crystallogr. Sect. A* **32,** 751 (1976).
11. National Center for Electron Microscopy Material and Chemical Sciences Divisions, Lawrence Berkeley Laboratory, "NCEMSS Program," University of California, 1989.